Deep-Sea Research I 111 (2016) 61–70

Contents lists available at ScienceDirect

Deep-Sea Research I

journal homepage: www.elsevier.com/locate/dsri

^{230}Th and ^{234}Th as coupled tracers of particle cycling in the ocean: A maximum likelihood approach

Wei-Lei Wang *[,1], Robert A. Armstrong, J. Kirk Cochran, Christina Heilbrun

School of Marine and Atmospheric Sciences, Stony Brook University, Stony Brook, NY, USA

ARTICLE INFO

Article history:
Received 29 June 2015
Received in revised form
31 January 2016
Accepted 5 February 2016
Available online 16 February 2016

Keywords:
Likelihood estimation
Sinking velocity
Thorium
Export flux
MedFlux

ABSTRACT

We applied maximum likelihood estimation to measurements of Th isotopes ($^{234,\ 230}$Th) in Mediterranean Sea sediment traps that separated particles according to settling velocity. This study contains two unique aspects. First, it relies on settling velocities that were measured using sediment traps, rather than on measured particle sizes and an assumed relationship between particle size and sinking velocity. Second, because of the labor and expense involved in obtaining these data, they were obtained at only a few depths, and their analysis required constructing a new type of box-like model, which we refer to as a "two-layer" model, that we then analyzed using likelihood techniques. Likelihood techniques were developed in the 1930s by statisticians, and form the computational core of both Bayesian and non-Bayesian statistics. Their use has recently become very popular in ecology, but they are relatively unknown in geochemistry.

Our model was formulated by assuming steady state and first-order reaction kinetics for thorium adsorption and desorption, and for particle aggregation, disaggregation, and remineralization. We adopted a cutoff settling velocity (49 m/d) from Armstrong et al. (2009) to separate particles into fast- and slow-sinking classes. A unique set of parameters with no dependence on prior values was obtained. Adsorption rate constants for both slow- and fast-sinking particles are slightly higher in the upper layer than in the lower layer. Slow-sinking particles have higher adsorption rate constants than fast-sinking particles. Desorption rate constants are higher in the lower layer (slow-sinking particles: 13.17 ± 1.61, fast-sinking particles: 13.96 ± 0.48) than in the upper layer (slow-sinking particles: $7.87\pm0.60\ y^{-1}$, fast-sinking particles: $1.81\pm0.44\ y^{-1}$). Aggregation rate constants were higher, 1.88 ± 0.04, in the upper layer and just $0.07\pm0.01\ y^{-1}$ in the lower layer. Disaggregation rate constants were just $0.30\pm0.10\ y^{-1}$ in the upper layer and higher, $3.01\pm0.35\ y^{-1}$, in the lower layer. For rapid-sinking particles, adsorption of Th from solution and aggregation of slow-sinking particles are the main source, and particle sinking is the main sink. For slow-sinking particles, adsorption is also the main source, but radioactive decay (for ^{234}Th) and desorption are the main sinks. Sinking and aggregation are small compared to adsorption and decay, and the contribution of disaggregation is negligible.

1. Introduction

The atmospheric concentration of CO_2 has been increasing since the Industrial Revolution as a result of the combustion of fossil fuels and land use changes (Siegenthaler and Sarmiento, 1993). The elevated atmospheric CO_2 concentration has induced climate changes because of the greenhouse effect (Barnett et al., 2005), and has resulted in ocean acidification because of dissolution of CO_2 in seawater (Doney et al., 2009). In the euphotic zone, phytoplankton use CO_2 to synthesize organic matter; some planktonic species also use dissolved inorganic carbon to produce their carbonate shells, which along with organic matter sink after the death of organisms due to their density excess over seawater.

Sinking particles play an important role in the "biological pump", which transports organic matter and carbonate particles from the surface water to the deep ocean (Volk and Hoffert, 1985). However, due to the high efficiency of heterotrophic remineralization, over 90% of the particulate organic carbon formed during photosynthesis in the surface waters is remineralized to inorganic forms in the upper ocean; only about 1% of surface-derived organic matter survives transit from the surface ocean to the deep sea and sediments (Wakeham and Lee, 1993; Feely et al., 2001).

Particle production, transportation, and remineralization have profound impacts on biogeochemical cycles of carbon and trace elements. Paradoxically, a few elements, such as thorium, which

* Corresponding author.
E-mail address: weileiw@uci.edu (W.-L. Wang).
[1] Current address: Department of Earth System Science, University of California at Irvine, CA 92697, USA.

http://dx.doi.org/10.1016/j.dsr.2016.02.003
0967-0637/

are strongly particle-reactive, provide an approach to studying how particles change during their downward transport, including the rates at which they aggregate and disaggregate (e.g., Nozaki et al., 1981; Honeyman and Santschi, 1989; Murnane et al., 1994, 1996) and the velocity at which they are sinking (e.g., Nozaki et al., 1981; Bacon and Anderson, 1982; Bourne et al., 2012). This is because thorium isotopes are easily adsorbed onto particle surfaces; when a particle experiences a transformation such as remineralization, aggregation, or disaggregation, thorium can be used to trace these changes.

When thorium isotopes (^{234}Th and ^{230}Th, with half-lives of 24.1 days and 75,380 years (Libes, 1992), respectively) are used together, they become significantly more valuable. The application of thorium isotopes to study marine biogeochemistry has evolved from a "single isotope application" to evaluate sediment trap efficiency (e.g., Fleisher and Anderson, 2003; Roy-Barman et al., 2009), and to calculate POC flux from the surface water (e.g., Santschi et al., 1979; Coale and Bruland, 1985; Buesseler, 1998), to a "multiple isotope application" to estimate particle aggregation, disaggregation, adsorption, desorption, and sinking rates (e.g., Cochran et al., 1993, 2000; Murnane, 1994; Murnane et al., 1994, 1996). The "multiple isotope application" has been implemented by creating box models that include dissolved thorium, plus large "sinking" and small "non-sinking" particulate thorium. In early publications (Clegg et al., 1991; Murnane et al., 1990, 1994, 1996; Cochran et al., 1993, 2000; Murnane, 1994; Marchal and Lam, 2012), a prior value of the sinking rate of large "sinking" particles was arbitrarily assigned. By contrast, in the MedFlux program that was conducted at the DYFAMED site (43° 25N, 7° 52E) in the Mediterranean Sea, *in situ* particle settling velocities were measured using an Indented Rotating Sphere (IRS) sediment trap in Settling Velocity (SV) mode (Peterson et al., 1993, 2009; Armstrong et al., 2009). With measured particle settling velocities, we can avoid the assumption that sinking velocity is determined only by particle size.

Previously published data on the depth distribution of ^{234}Th in MedFlux SV traps (Szlosek et al., 2009) (Fig. 1), showed that slow-sinking particles (SV less than $\leq$ 49 m/d) had ^{234}Th fluxes that were approximately the same in shallow and deep traps, while ^{234}Th fluxes in fast-sinking particles were higher in deep than in shallow traps. The box model applied by Szlosek et al. (2009) to the data suggested two possibilities to explain the pattern: 1) additional adsorption of ^{234}Th onto the slow-sinking particles at a rate balanced by radioactive decay, plus additional adsorption of ^{234}Th onto the fast-sinking particles with minimal decay because of the rapid sinking rate or, 2) aggregation and disaggregation between the SV classes that transferred ^{234}Th among them at rates sufficient to explain the data. Here we present new data on ^{230}Th for the same samples and use a maximum likelihood approach to assess which process(es) is (are) responsible for the pattern.

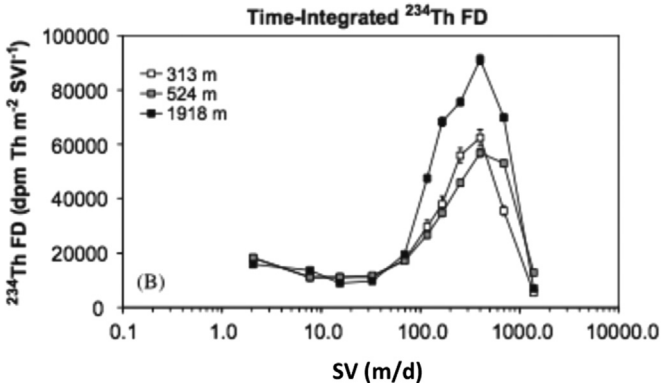

Fig. 1. Time-integrated ^{234}Th flux density (FD) versus settling velocity (SV) at three different depths: SV2 at 313 m, mass average of SV1 and SV2 at 524 m and 1918 m. Note: There were two SV traps at each depth: designated SV1, SV2. At 313 m SV1 did not work, and therefore only data from SV2 are available (Reproduced from Szlosek et al. (2009)).

2. Methods

2.1. Sediment trap operation

In 2005, the MedFlux program deployed a sediment trap array with Indented Rotating Sphere (IRS) traps operated in the Settling Velocity (SV) mode (as opposed to the time-series mode) in the Mediterranean Sea. A full description of IRS-SV sediment trap operation was presented by Peterson et al. (1993, 2005, 2009). Briefly, the bottom-tethered sediment trap array was deployed for 55 days in 2005, with actual sampling depths of 313 m, 524 m, and 1918 m. Sinking particles are first captured by a cylindrical particle interceptor; they then fall onto an indented sphere that rotates on a programmed time schedule. The rotation of the sphere transfers the particles into a skewed funnel that leads to a sampling carousel, in which there are 12 sampling tubes. The carousel is programmed to rotate at particular times, and particles with different settling velocities settle into different tubes. The first sampling position has no sampling cup and is open during deployment and retrieval of the trap; therefore, only 11 settling velocity categories are measured. The full data set is available online at: http://www.somassbu.org/research/medflux/. The mass fluxes and settling velocities of the different fractions are given in Table 1.

2.2. Radionuclide analyses

Two SV traps were deployed at each of three depths (313, 524, and 1918 m) during the 2005 MedFlux program. Following trap recovery, samples were split and aliquots for radionuclide measurement were filtered onto single 25-mm 0.4 μm Nuclepore filters. The filters were initially mounted for non-destructive beta counting to determine ^{234}Th activities, as described in detail by Szlosek et al. (2009). Following beta counting the filters were analyzed radiochemically. They were dissolved in 1.5N HCl and ^{210}Po was plated onto silver discs and stored for a second plating of ingrown ^{210}Po to determine ^{210}Pb. The solution was then evaporated to near dryness and re-dissolved in 8N HNO_3, then evaporated and re-dissolved in Aqua Regia, and finally evaporated and re-dissolved in 8N HCl in preparation for radiochemical separation of Th using Dowex 1-X8 100–200 mesh anion exchange resin. ^{229}Th was used as a yield tracer. Columns were prepared with 5 ml of resin and conditioned with 8N HCl. The sample was added to the column and the Th fraction was eluted with 8N HCl. This was taken to near dryness and re-dissolved in a mixture of HCl and HNO_3 before it was evaporated and re-dissolved in 8N HNO_3. A second column with the same resin and conditioned with 8N HNO_3 was used to separate Ra and Th. Th was eluted with 8N HCl and this solution was taken to dryness and redissolved in 1.5N HCl.

The purified Th fractions were plated onto stainless steel discs for alpha spectrometry. Sample activities of ^{232}Th, ^{230}Th, and ^{228}Th were measured. Here we present only the ^{232} Th and ^{230}Th data because we could not precisely determine the contribution to the ^{228}Th peak of ^{228}Th ingrown from any ^{228}Ra taken up by the particles (Table 1). Of the two SV traps deployed at each depth, Th isotope activities were determined on one trap series from 313 m (SV2; Table 1) and a mass-weighted average of the two trap series from 524 m (SV1, SV2; Table 1). At 1918 m, the individual sample solutions from the two trap series were combined because the relatively low activities required long counting times, and the final rate was estimated by dividing the measured activities in half

Table 1
Radionuclide and mass data from MedFlux 2005 settling velocity sediment traps.

Depth (m)	Trap ID	Mass flux[a] ($g/m^2/d$)	Minimum SV[a] (m/d)	Midpoint SV[a] (m/d)	^{234}Th[b] (dpm/g)	^{234Th} Flux[2] ($dpm/m^2/d$)	^{230}Th (dpm/g)	^{232}Th (dpm/g)	$^{230}Th_{xs}$[c] (dpm/g)	$^{230}Th_{xs}$ flux ($dpm/m^2/d$)
313	***SV2 02A***	5.96	980	1200	4494 ± 576	26.8	2.99 ± 0.51	0.99 ± 0.26	2.42	0.014
	SV2 03A	62.22	490	734.4	2803 ± 146	174.4	3.50 ± 0.32	3.32 ± 0.32	1.61	0.100
	SV2 04A	75.38	326	408.0	2375 ± 130	179.0	1.11 ± 0.14	0.92 ± 0.13	0.59	0.044
	SV2 05A	80.49	196	261.1	2511 ± 138	202.1	2.09 ± 0.19	2.27 ± 0.20	0.80	0.064
	SV2 06A	39.30	140	167.9	2301 ± 199	90.4	1.99 ± 0.25	2.87 ± 0.32	0.36	0.014
	SV2 07A	29.75	98	118.9	2517 ± 231	74.9	2.39 ± 0.27	2.10 ± 0.27	1.20	0.036
	SV2 08A	26.71	49	73.5	3200 ± 252	85.5	4.44 ± 0.32	2.16 ± 0.22	3.21	0.086
	SV2 09A	23.22	22	35.4	2763 ± 273	64.2	2.05 ± 0.22	2.04 ± 0.23	0.88	0.021
	SV2 10A	21.83	11	16.4	2517 ± 283	55.0	2.28 ± 0.23	1.60 ± 0.20	1.36	0.030
	SV2 11A	20.91	5	8.2	2594 ± 313	54.2	3.51 ± 0.51	0.25 ± 0.10	3.36	0.070
	SV2 12A	88.74	0.68	3.1	3028 ± 111	268.7	1.95 ± 0.19	0.74 ± 0.12	1.52	0.135
524	***SV1 02A***	33.79	980	1200	2389 ± 86	80.7	2.23 ± 0.18	2.43 ± 0.20	0.85	0.029
	SV1 03B	127.75	490	734.4	2279 ± 41	291.2	2.28 ± 0.19	2.05 ± 0.18	1.11	0.142
	SV1 04B	51.63	326	408.0	2804 ± 77	144.8	3.13 ± 0.37	2.50 ± 0.34	1.70	0.088
	SV1 05A	55.22	196	261.1	2703 ± 76	149.2	1.58 ± 0.14	2.15 ± 0.17	0.36	0.020
	SV1 06A	22.38	140	167.9	2710 ± 122	60.6	3.88 ± 0.32	2.76 ± 0.27	2.31	0.052
	SV1 07A	17.74	98	118.9	2872 ± 153	51.0	1.91 ± 0.26	1.70 ± 0.26	0.94	0.017
	SV1 08B	18.50	49	73.5	3072 ± 149	56.8	4.76 ± 0.41	1.98 ± 0.26	3.63	0.067
	SV1 09B	16.05	22	35.4	3098 ± 170	49.7	2.68 ± 0.29	2.36 ± 0.28	1.33	0.021
	SV1 10B	16.98	11	16.4	2835 ± 161	48.1	1.83 ± 0.23	2.81 ± 0.32	0.23	0.004
	SV1 11B	22.28	5	8.2	3290 ± 163	73.3	14.60 ± 1.09	8.71 ± 0.85	9.63	0.215
	SV1 12B	88.76	0.68	3.1	2996 ± 78	265.9	0.98 ± 0.14	0.61 ± 0.11	0.63	0.056
	SV2 02B	13.68	980	1200	3308 ± 227	45.3	4.77 ± 0.95	5.73 ± 1.00	1.50	0.021
	SV2 03B	100.3	490	734.4	2297 ± 65	230.4	2.08 ± 0.12	2.06 ± 0.16	0.91	0.091
	SV2 04B	71.64	326	408.0	2527 ± 76	181.1	1.68 ± 0.33	1.43 ± 0.35	0.87	0.062
	SV2 05B	78.33	196	261.1	2336 ± 72	183.0	2.62 ± 0.14	1.60 ± 0.10	1.70	0.134
	SV2 06B	48.45	140	167.9	2172 ± 90	105.2	3.08 ± 0.29	1.81 ± 0.12	2.05	0.099
	SV2 07B	32.05	98	118.9	2625 ± 136	84.1	1.88 ± 0.19	2.32 ± 0.18	0.56	0.018
	SV2 08B	34.48	49	73.5	3270 ± 111	112.7	2.11 ± 0.19	1.91 ± 0.20	1.02	0.035
	SV2 09B	23.65	22	35.4	3613 ± 138	85.4	2.25 ± 0.16	2.26 ± 0.19	0.96	0.023
	SV2 10B	19.30	11	16.4	3157 ± 151	60.9	3.18 ± 0.23	2.47 ± 0.24	1.77	0.034
	SV2 11B	11.29	5	8.2	3201 ± 177	36.1	11.05 ± 0.18	2.95 ± 0.09	9.37	0.106
	SV2 12B	93.25	0.68	3.1	2901 ± 64	270.5	2.27 ± 0.15	2.09 ± 0.14	1.08	0.101
1918	**SV1+2#2**	16.16	980	1200	3131 ± 346	50.6	5.69 ± 0.56	2.54 ± 0.26	4.24	0.069
	SV+2#3	102.84	490	734.4	3407 ± 62	350.4	1.04 ± 0.11	1.87 ± 0.20	−0.03	−0.003
	SV1+2#4	76.39	326	408.0	3532 ± 74	269.8	1.60 ± 0.07	1.49 ± 0.07	0.75	0.057
	SV1+2#5	73.23	196	261.1	3758 ± 75	275.2	1.25 ± 0.14	1.85 ± 0.30	0.20	0.015
	SV1+2#6	39.83	140	167.9	4202 ± 110	167.4	1.25 ± 0.22	1.47 ± 0.13	0.41	0.016
	SV1+2#7	30.08	98	118.9	4227 ± 104	127.2	3.26 ± 0.38	2.01 ± 0.28	2.11	0.064
	SV1+2#8	21.43	49	73.5	4569 ± 148	97.9	4.04 ± 0.42	1.90 ± 0.28	2.96	0.063
	SV1+2#9	13.29	22	35.4	4254 ± 201	56.5	2.87 ± 0.55	1.30 ± 0.14	2.13	0.028
	SV1+2#10	10.21	11	16.4	4349 ± 234	44.4	7.95 ± 0.39	2.88 ± 0.23	6.31	0.064
	SV1+2#11	16.24	5	8.2	4435 ± 190	72.0	3.11 ± 0.32	2.77 ± 0.33	1.53	0.025
	SV1+2#12	53.07	0.68	3.1	4432 ± 100	235.2	0.49 ± 0.12	0.71 ± 0.09	0.09	0.005

[a] Lee et al. (2009) and Armstrong et al. (2009).
[b] Szlosek et al. (2009).
[c] Excess ^{230}Th, calculated as $^{230}Thxs = ^{230}Th - (0.57 \times ^{232}Th)$ (Bacon, 1984).

(SV1+SV2; Table 1). Uncertainties presented in Table 1 are 1 standard deviation and were derived from both sample and background count rates.

2.3. Model of thorium and particle cycling

In previous studies, models used to describe Th-particle cycling were either based on particulate Th data sampled (i) by large volume pumps that sort particles according to their size (Nozaki et al., 1987; Marchal and Lam, 2012), or (ii) a combination of pumps and sediment traps (Murnane et al., 1990, 1994, 1996). The model based solely on pump data had three phases: a dissolved phase, small particles, and large particles. It was assumed that large particles did not interact with the dissolved phase directly, but rather through small particles that were assumed to be "non-sinking". The model based on both pump and sediment trap data has nearly the same structure as that based only on pump data, but the "large" or "sinking" particles were also sampled using sediment traps.

The previous models had at least three disadvantages. First, the assumption that small particles do not sink is weak. As reported in McDonnell and Buesseler (2010), the plots of sinking velocity versus particle size may sometimes have "U-shaped" distributions; particle sinking velocity sometimes does not depend on particle size in a straightforward manner. Therefore, the assumption that small particles are "non-sinking" may be inappropriate. Second, particles caught by a large-volume pump may be a combination of "non-sinking" particles and "sinking" particles, whereas particles retained on the small pore size filter are deemed "non-sinking" particles. The third disadvantage is that the prior sinking velocities that some authors assigned to large particles (100 m/d in Nozaki et al. (1987), and 150 m/d in other references (Murnane et al., 1990, 1994, 1996; Marchal and Lam, 2012) might be lower than the actual particle sinking speed. For example, Armstrong et al. (2009) reported an average sinking velocity of 353±76 m/d for the fast-sinking fraction by modeling data obtained from settling velocity sediment traps. Using a different method, Xue and Armstrong (2009) gave added support to values higher than 150 m/d and reported that particles at the DYFAMED site sank at an average velocity of 220 m/d. The fact that the likelihood method does not require prior estimates of sinking velocities eliminates this possible source of bias.

Here we consider a model describing the cycling of particles and thorium in two layers whose interfaces coincide with the depths of the SV sediment traps deployed in 2005 at the DYFAMED site. Thus, the upper layer extends from 313 to 524 m, and the lower layer extends from 524 to 1918 m. We assume that in each layer the sinking flux of particles or of particulate thorium, $f_i(z)$, varies linearly with depth, z (counted positive downwards):

$$f_i(z) = \frac{(z_{bot} - z)f_i(top) + (z - z_{top})f_i(bot)}{z_{bot} - z_{top}} \quad (1)$$

where z_{bot} *and* z_{top} are depths of the bottom and top of the layer, respectively. We divide each flux, $f_i(z)$, by its corresponding geometrically averaged settling velocities (Armstrong et al., 2009) to estimate the concentration of particles, of particulate ^{230}Th, or of particulate ^{234}Th

$$C_i(z) = \frac{(z_{bot} - z)C_{top} + (z - z_{top})C_{bot}}{z_{bot} - z_{top}} \quad (2)$$

The model used in this study (Figs. 2 3) is almost identical to that used by Murnane (1994), Murnane et al. (1994, 1996), and

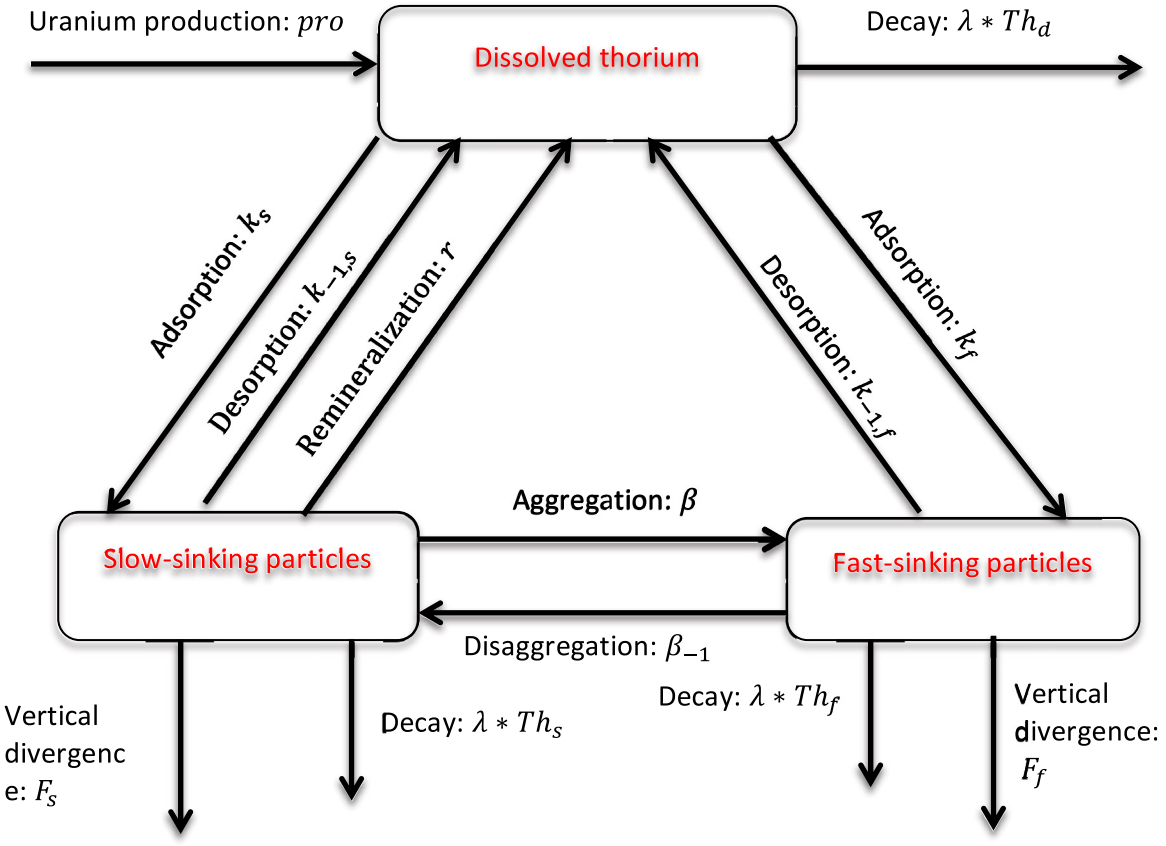

Fig. 2. "Two-layer" model describing thorium cycling. Dissolved thorium interacts with particulate thorium via adsorption, desorption, and remineralization of slow-sinking particles. In addition, dissolved thorium has a source from uranium radioactive decay and is lost via radioactive decay. Thorium on different sinking classes is exchanged via particle aggregation and disaggregation. Particulate thorium is lost through radioactive decay, vertical divergence, and desorption, and is gained by adsorption.

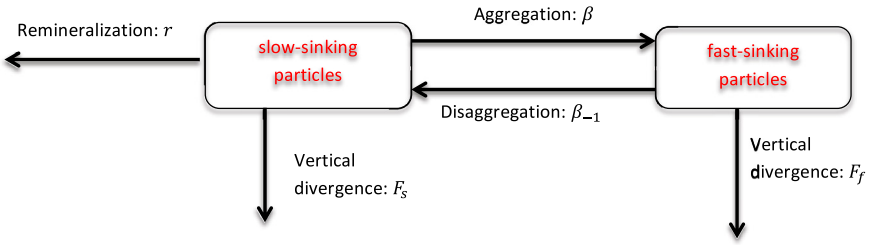

Fig. 3. "Two-layer" model describing particle cycling. Slow-sinking particles can form fast-sinking particles by aggregation; and fast-sinking particles can disaggregate to form slow-sinking particles. Slow-sinking particles are also lost by remineralization, which is ignored for fast-sinking particles.

Marchal and Lam (2012), except that we separate particles into sinking velocity classes. It relies on samples collected using IRS SV sediment traps and has the advantage that particle sinking velocities were measured directly by the SV traps, avoiding the need to arbitrarily assign prior values for sinking rates for "large" particles. Additionally, since particles were separated by sinking speed instead of particle size, we have a direct measure of sinking velocity for "slow-sinking" particles, and do not need to rely on the assumption that "small" particles are "slow", and that "slow" means "non-sinking".

In applying the two-layer model of Fig. 2, we incorporate thorium exchange between the dissolved phase and fast- and slow-sinking via adsorption and desorption, but ignore remineralization of fast-sinking particles. Specifically, dissolved ^{230}Th and ^{234}Th are produced from the radioactive decay of uranium and removed by radioactive decay. Dissolved thorium is also lost by adsorption onto sinking particles, and is added to solution by desorption from particles and remineralization from the slow-sinking particles. For these particles, ^{230}Th and ^{234}Th are lost by radioactive decay, desorption, and particle remineralization, aggregation, and sinking (when the sinking flux divergence is negative), and are added by adsorption and fast-sinking particle disaggregation. For the fast-sinking class, thorium is lost by radioactive decay, desorption, and disaggregation, and added by adsorption and the aggregation of slow-sinking particles. All interactions are assumed to have first-order reaction kinetics. All rate constants are assumed to be constant in a given layer, but are allowed to vary between the two layers.

In steady state, the difference in the flux at the top and bottom of a layer is balanced by the sum of the processes taking place in the layer,

$$f_{i,bot} - f_{i,top} = \sum (\varnothing_{i,j}) \tag{3}$$

where $\varnothing_{i,j}$ is the contribution from jth process in the ith SV class. For example, the contribution of adsorption in the settling velocity category of i is as follows,

$$\varnothing_{i,adsorption} = \int_{top}^{bot} (k_1 \times Th_{d,z})\,dz \tag{4}$$

where k_1 is the adsorption rate constant, and $Th_{d,z}$ is the dissolved thorium concentration at depth z. We substitute $Th_{d,(z)}$ given by Eq. (2) into Eq. (4) and then integrate Eq. (4) to obtain the following equation.

$$\varnothing_{i,adsorption} = 0.5 \times k_1 \times \left[(Th_{d,top} + Th_{d,bot}) \times (z_{bot} - z_{top}) - (Th_{d,top} - Th_{d,bot}) \times z_{top} \right]$$

where $Th_{d,top}$ and $Th_{d,bot}$ are the dissolved thorium isotope concentrations at the top and at the bottom of a layer, respectively. All the other processes have the same format.

As shown by Armstrong et al. (2009), in this data set there were 4 settling velocity intervals that fell into the slow-sinking classes, and the other 7 intervals were in the fast-sinking classes. Therefore, the total contribution of adsorption to slow sinking class is

$$\Phi_{s,adsorption} = \sum_{i=1}^{4} \varnothing_{i,adsorption} \tag{5}$$

Then the balance equation for thorium on slow-settling particles is:

$$\Delta F_{Th,s} = \Phi_{s,adsorption} - \Phi_{s,desorption} + \Phi_{f,disaggregation} - \Phi_{s,aggregation} - \Phi_{s,decay} - \Phi_{s,remineraization} \tag{6}$$

For thorium on fast-settling particles, the equation is:

$$\Delta F_{Th,f} = \Phi_{f,adsorption} - \Phi_{f,desorption} + \Phi_{s,aggregation} - \Phi_{f,disaggregation} - \Phi_{f,decay} \tag{7}$$

where $\Delta F_{Th,s}$, $\Delta F_{Th,f}$ are the left sides of Eq. (3) for particulate thorium in slow- and fast-sinking classes, respectively.

For dissolved thorium, the equation is:

$$\Phi_{u,production} - \Phi_{d,decay} = \Phi_{f+s,adsorption} - \Phi_{f+s,desorption} - \Phi_{s,remineralization} \tag{8}$$

where $-\Phi_{f+s,\ldots}$ reflects contributions from both fast and slow sinking particles, $\Phi_{u,production}$ $(\lambda \times U)$ reflects a source from uranium decay, and $\Phi_{d,decay}$ $(\lambda \times Th)$ means a loss from thorium decay. λ is the thorium decay constant, and U and Th are observed dissolved uranium and thorium activity, respectively.

The following two equations describe particle cycling:

$$\Delta F_{p,s} = \Phi_{f,disaggregation} - \Phi_{s,aggregation} - \Phi_{s,remineraization} \tag{9}$$

$$\Delta F_{p,f} = \Phi_{s,aggregation} - \Phi_{f,disaggregation} \tag{10}$$

where $\Delta F_{p,s}$ and $\Delta F_{p,f}$ are left-hand sides of Eq. (3) for slow- and fast-sinking particles, respectively.

2.4. Radionuclide data applied to the model

Estimates of dissolved and particulate activities of ^{234}Th and ^{230}Th and their respective parents, ^{238}U and ^{234}U, are needed for application of the model presented in Section 2.3. The distribution of ^{238}U has been measured at the DYFAMED site, and was reported by Cochran et al. (2009). ^{238}U was uniformly distributed at the depths studied here (313–1918 m); and a constant value of 2700 dpm/m^3 is therefore used. This value is also consistent with the relationship between salinity and ^{238}U (Owens et al., 2011) at a salinity of 38, typical of the Mediterranean Sea. The activity of ^{234}U was calculated based on the relationship $^{234}U = 1.14 \times ^{238}U = 1.14 \times 2700 = 3078$ dpm/m^3 (Chen et al., 1986).

In contrast to uranium, thorium (^{234}Th and ^{230}Th) activities both in solution and on sinking particles vary with depth. The activities of dissolved ^{234}Th are from Cochran et al. (2009), who calculated dissolved ^{234}Th during the MedFlux project by taking the difference between total ^{234}Th and particulate ^{234}Th, as sampled by Niskin bottles and Challenger Oceanic battery-operated *in-situ* pumps, respectively. However, dissolved ^{234}Th was not

measured at the exact trap depths of 313, 524, and 1918 m. At 313 m, dissolved ^{234}Th concentration was therefore linearly interpolated using the data sampled at 200 m and 400 m on March 13, 2005; at 524 m, ^{234}Th concentration was linearly interpolated using the data sampled at 400 m and 600 m on March 9, 2005; at 1918 m, dissolved ^{234}Th was taken as the data sampled at 1800 m on March 9, 2005, because no deeper data were available. Based on interpolation and extrapolation that are described above, the activities of dissolved ^{234}Th are 2518 dpm/m^3 at 313 m, 2469 dpm/m^3 at 524 m, and 2520 dpm/m^3 at 1918 m. The activities of dissolved ^{230}Th were taken from measurements reported by Roy-Barman et al. (2002), who sampled at the DYFAMED site at the end of the summer of 1996. After unit conversion from fg/kg(used in Roy-Barman et al. (2002)) to dpm/m^3, the activities of dissolved ^{230}Th are 0.13 dpm/m^3 at 313 m (interpolating values at 200 m and 500 m), 0.16 dpm/m^3 at 524 m (taken as the value measured at 500 m), and 0.17 dpm/m^3 at 1918 m (interpolating values at 1500 m and 2000 m). Particulate ^{234}Th and ^{230}Th were collected using the SV sediment traps, therefore, no interpolation or extrapolation was needed for them.

2.5. Theory and algorithm of the likelihood method

Technically, if the difference between a data point (y_i) and the model prediction ($\hat{y}_i$) of that value is normally distributed with variance σ^2, then for that data point the best choice of parameters will be the one that maximizes

$$L(y_i) = \frac{1}{\sqrt{(2\pi\sigma^2)}} \times \exp\left(- \frac{\left(y_i - \hat{y}_i\right)^2}{2\sigma^2} \right) \tag{11}$$

If we have n data points and assume constant variance (σ^2), according to Hilborn and Mangel, (1997) the quantity to be maximized will be

$$L(y_i \cdots y_n) = \prod_{i=1}^{n} \left[\frac{1}{\sqrt{(2\pi\sigma^2)}} \times \exp\left(- \frac{\left(y_i - \hat{y}_i\right)^2}{2\sigma^2} \right) \right] \tag{12}$$

The natural logarithm of Eq. 12 is

$$ln(L(y_i \cdots y_n)) = - \frac{n}{2} \times ln\left[2\pi\sigma^2\right] - \sum_{i=1}^{n} \frac{\left(y_i - \hat{y}_i\right)^2}{2\sigma^2} \tag{13}$$

Finally, we substitute σ^2 in Eq. 13 with $(\sigma^2 = \frac{1}{n} \times \sum_{i=1}^{n} (y_i - \hat{y}_i)^2)$ and eliminate the "nuisance parameter" (Edwards, 1992), leading to

$$\ln L = - \left(\frac{n}{2}\right) \times \ln\left(\frac{\sum_{i=1}^{n} \left(y_i - \hat{y}_i\right)^2}{n} \right) \tag{14}$$

By maximizing likelihood, we are trying to find a set of parameters that has the highest probability of having produced the data in a sense that minimizes the difference between model predictions ($\hat{y}_i$) and measurements (y_i), thus highest likelihood. That set of parameters is called the maximum likelihood estimate (MLE) (Hilborn and Mangel, 1997).

In our study, the large differences in concentrations between ^{234}Th and ^{230}Th lead to great differences in their "error variances" ($\sigma^2 = \frac{1}{n} \times \sum_{i=1}^{n} (y_i - \hat{y}_i)^2$); these variances were calculated after we obtained the model prediction ($\hat{y}_i$, which are left-sides of (Eqs. (6)–10)). We present them here to prove the necessity of using separated likelihoods for particles, ^{234}Th, and ^{230}Th. For example, the standard deviation (SD, square root of variance) of ^{234}Th in the study area is about 3.04×10^2 dpm m^{-3} y^{-1}; the SD of particle mass is about 60.18 mg m^{-3} y^{-1}, whereas the SD of ^{230}Th is about 2.83×10^{-2} dpm m^{-3} y^{-1}. The large differences in variances apparently violate the assumption that the variance is constant. However, since likelihoods ($\mathcal{L}$) are derived from probabilities and are proportional to the probability of hypothesis *(H)* given data (*data1, data2, data3,* ⋯), likelihoods are multipliable:

$$\mathcal{L}\{Hdata1, data2, data3, \cdots\} = \mathcal{L}\{Hdata1\} \times \mathcal{L}\{Hdata2\} \times \mathcal{L}\{Hdata3\} \times \cdots, \tag{15}$$

and logarithms of likelihoods can be factorized:

$$Ln\, L\{Hdata1, data2, data3, \cdots\} = \ln L\{Hdata1\} + \ln L\{Hdata2\} + \ln L\{Hdata3\} + \cdots \tag{16}$$

where data1, *data2, and data3* in the current study represent differences in the fluxes and/or differences in decay production and loss of particulate ^{230}Th, particulate ^{234}Th, and particles, respectively. The hypothesis *(H)* here is defined as the model prediction. This feature of likelihood enables us to include different types of data in a single framework (Hilborn and Mangel, 1997). We calculated log-likelihood separately for ^{234}Th, ^{230}Th, and particles, allowing each to have its own variance, then added them together to get a total log-likelihood, which was maximized using a simulated annealing algorithm (Metropolis et al., 1953; Press et al., 1986; Armstrong et al., 2002). This algorithm finds model parameters that maximize the probability that the given data were obtained. An initial value and a boundary are needed for each parameter. Parameters are randomly generated within their boundaries during each iteration. The code is designed to avoid the possibility that the algorithm is trapped in local minima. The way that the algorithm is designed enables it to be independent of the initial guess. A half-million iterations were used to find the best parameter values for the model.

We should note that our likelihood parameter estimates are best fits, and that their associated variances do not apply to individual parameters, but only to the three classes of data (^{234}Th, ^{230}Th, and particles). The variance values represent not only counting errors, but also variance introduced by trap or ship positioning, water movements, seasonality (after all, the traps were employed for 55 days!), and other factors, and so represent a true picture of total system variability.

2.6. Parameter sensitivity

To study parameter sensitivity alone, we contaminated the original data with random errors that were consistent with measurement errors. We used relative errors of 1% for particle mass and 5% for ^{234}Th activity. Relative error for ^{230}Th$_{ex}$ was estimated to be 17% based on ^{230}Th and ^{232}Th measurement errors and the relationship of ^{230}Thxs=^{230}Th−(0. 57 × ^{232}Th). We ran the model a hundred times, each time with different random errors. We then calculated standard error as shown in Table 2 based on the total runs.

3. Results

3.1. Division of fast and slow-sinking classes

To decrease the number of parameters, we divided the 11 SV categories separated by SV sediment traps into two sinking classes. The SV division (SVD) we used is obtained from Armstrong et al. (2009), in which time-averaged mass flux density versus settling velocity have two sets of clearly different distributions. Fluxes in

Table 2
Summary of rate constants estimated by thorium isotopes. Remineralization rate constants estimated for slow-sinking particles in this study are 1.74×10^{-3} y^{-1} between 313 and 524 and 0.50 y^{-1} between 524 and 1918, respectively. Remineralization is ignored for fast-sinking particles.

References	Site	Adsorption (y^{-1})	Desorption (y^{-1})	Aggregation (y^{-1})	Disaggregation (y^{-1})
Lavelle et al. (1991)	Puget sound	10–42	316	50±3–90±20	90±15–630±190
Nozaki et al. (1987) particulate data	Western Pacific	0.20±0.27–0.44±1.2	0.88±1.2–1.89±5.1	2.36±5.9–12.3±213	148±370–788±1400
Nozaki et al. (1987) total data	Western Pacific			0.18	62
				0.14±0.01	50±5
Nozaki et al.(1987) total and particulate data	Western Pacific			0.11±0.03	16±9
Bacon et al. (1989)	Arctic Ocean	0.16–0.47	2.6–9.8		
Bacon and Anderson (1982)	Panama Basin	0.2–1.3	1.3–6.3		
Nozaki et al. (1981)	Pacific Ocean	1.5	6.3		
Clegg et al. (1991)	Equatorial Pacific	1–4	2.5±1.0	<0.1–50	<50–>365
	North Pacific	3–70	2.5±1.0	<1–~40	~65
	North Pacific, range below 100 m	1–3	2.5±1.0	~0.7	~65
Clegg and Whitfield (1991)		0.2–2.6	1.8	3.7–640	15–6500
Murnane et al. (1990)	North Pacific	0.5±1.0	1.0±0.1	0.2±0.01	0.8±0.2
Cochran et al. (1993)	North Atlantic (^{234}Th)	–	–	1.1–33	126–407
	North Atlantic (^{228}Th)	–	–	−0.5 to 20	108–281
Cochran et al. (2000)	Ross SEA, S. ocean	–	–	0.04–0.2	2.4–13.8
This study 313–524 m	DYFAMED	0.16±0.004 (f)–1.43±0.04 (s)	1.81±0.44(f)–7.87±0.60 (s)	1.88±0.04	0.30±0.08
This study 524–1918 m	DYFAMED	0.14±0.001(f)–1.39±0.10 (s)	13.17±1.61(s)–13.96±0.48(f)	0.07±0.01	3.01±0.35

the four slowest SV categories have an exponential distribution. Fluxes in the rest of the SV categories have a Gaussian distribution. These two functions were fit to the data using likelihood (Armstrong et al., 2009). All the calculations here are based on this SVD.

3.2. Model parameters (adsorption, desorption, aggregation, disaggregation, and remineralization)

Estimated parameter values were calculated using an annealing algorithm, which is coded in Matlab. Optimized parameters together with reference reported values are shown in Table 2. Adsorption rate constants of slow-sinking particles estimated in the upper and lower layers are 1.43 ±0.04 y^{-1} to 1.39 ±0.10 y^{-1}, respectively. Adsorption rate constants of the fast-sinking particles are ~10 times lower than that of slow-sinking particles. Thorium desorption rate constants estimated in the upper layer are lower than in the lower layer. An interesting finding is that slow-sinking particles have both higher desorption and adsorption rate constants compared to fast-sinking particles. Remineralization rate constants were estimated to be 1.74×10^{-3} y^{-1} in the upper layer, and 0.50±0.01 y^{-1} in the lower. Aggregation rate constants in the upper layer are higher than in the lower layer, and disaggregation rate constants show an opposite trend. Generally, disaggregation and desorption rate constants are more sensitive to data errors

Table 3
The source and sink terms for ^{234}Th (upper) and ^{230}Th (lower). A negative sign before a number indicates a sink; a positive number indicates a source. (Units: dpm/m^3/y)

	Top layer (313–524 m)			Bottom layer (524–1918 m)		
	Dissolved	Fast	Slow	Dissolved	Fast	Slow
A) For ^{234}Th						
Decay[a]	2556.3	−42.4	−1519.6	1851.2	−58.2	−1486.4
Adsorption	−3543.1	431.0	3112.1	−3745.0	318.9	3426.1
Desorption	986.6	−0.1	−986.5	1818.4	−42.1	−1776.3
Remineralization	0.2	–	−0.2	75.4	–	−75.4
Sinking flux		−622.7	−371.6		−208.8	−97.8
Aggregation		234.3	−234.3		27.0	−27.0
Disaggregation		−0.1	0.1		−36.8	36.8
SUM	**0.00**	**0.00**	**0.00**	**0.00**	**0.00**	**0.00**
B) For ^{230}Th						
Decay[a]	0.020	0.000	0.000	−0.012	0.000	0.000
Adsorption	−0.278	0.034	0.243	−0.251	0.021	0.230
Desorption	0.257	−0.000	−0.257	0.253	−0.015	−0.238
Remineralization	0.000	–	−0.000	0.010	–	−0.010
Sinking flux		−0.095	0.074		−0.056	0.036
Aggregation		0.061	−0.061		0.038	−0.038
Disaggregation		−0.000	0.000		−0.000	0.000
SUM	**0.000**	**0.000**	**0.000**	**0.000**	**0.000**	**0.000**

[a] For the dissolved phase, “decay” means the difference of uranium radioactive decay production and thorium radioactive decay loss; for particulate thorium (fast and slow sinking particles), “decay” means loss via radioactive decay.

than adsorption rate constants (Table 2).

3.3. Processes that influence the balance of ^{234}Th

Source and sink terms for ^{234}Th are displayed in Table 3**(A)**. The main source of dissolved ^{234}Th is the production from ^{238}U radioactive decay; its main sink is radioactive decay. The contributions of these two processes to the ^{234}Th mass balance are much higher than those from particle adsorption and desorption. For fast-sinking particulate ^{234}Th, loss through radioactive decay is relatively small, which is consistent with our expectation that a fast sinking speed leaves little time for radioactive decay. The major loss by vertical flux divergence is compensated by adsorption and aggregation from slow-sinking particles. Slow-sinking particulate ^{234}Th, due to its low sinking speed and long transition time, is mainly lost through radioactive decay and desorption, which are mainly balanced by adsorption. The loss by remineralization increases with depth, but overall its contribution is small. Aggregation of slow-sinking particles to fast-sinking particles is significant compared to disaggregation.

3.4. Processes that dominate the balance of ^{230}Th

The source and sink terms for ^{230}Th are displayed in Table 3**(B)**. For all three phases, the loss from radioactive decay is negligible due to its long half-life. For dissolved ^{230}Th, the source is primarily desorption and the major sink is adsorption onto particles. For fast-sinking particulate ^{230}Th, in both layers, aggregation and adsorption together compensate for the loss by vertical transport. For slow-sinking particulate ^{230}Th, adsorption is constantly a major source in both layers, and desorption is the major sink. In both layers, losses via remineralization are small enough to be ignored.

4. Discussion

4.1. Comparison with prior work

4.1.1. Adsorption rate constants

To our knowledge, this is the first study that applies a model of multiple thorium isotopes on particles that were separated into fast- and slow-sinking classes instead of large and small classes. It is also the first study that allows direct interactions between dissolved thorium and fast-sinking particles. Therefore, there is no reference available for us to make a side-by-side comparison. However, estimates of adsorption and desorption rate constants do exist, although different methods were used to obtain them. For example, Murnane et al. (1990) reported adsorption rate constants of 0.47 y^{-1} at Station P and 0.19–0.44 y^{-1} in the western Pacific. Bacon et al. (1989) reported adsorption rate constants ranging from 0.16 to 0.47 y^{-1} at the Arctic Ocean. Bacon and Anderson (1982) reported estimates of 0.2–1.3 y^{-1} at the Panama Basin. Adsorption rate constants for slow-sinking particles in this paper range from 1.39 ± 0.10 to 1.43 ± 0.04 y^{-1}, which is in good agreement with these studies. For fast-sinking particles, adsorption rate constants range from 0.14 ± 0.001 to 0.16 ± 0.004 y^{-1}, which are at the lower end of reported values.

Our estimates of adsorption rate constants for fast-sinking particles are an order of magnitude lower than those for slow-sinking particles. We offer one explanation. Particle composition could have an impact on thorium adsorption rate. Analysis of particles collected in the MedFlux project in the slow- and fast-sinking classes (Table 4) shows that slow-sinking particles have consistently higher organic matter content than fast-sinking particles at all three depths. Other components of the particulate matter do not show a consistent pattern. Organic matter can enhance thorium adsorption onto particles (Quigley et al., 2002; Santschi et al., 2006; Chuang et al., 2014), so that it is possible that the lower organic matter content of fast-sinking particles results in lower adsorption rate constants. Additionally, the predicted pattern that adsorption rate constants are higher in the upper layer than the lower layer is consistent with the organic matter depth distribution trend.

Table 4
Particle compositions for fast- and slow-sinking classes (Reproduced from Lee et al. (2009)).

Depth (m)	Organic matter (mg/g)	Lithogenic (mg/g)	Opal.H_2O (mg/g)	$CaCO_3$ (mg/g)
313				
Fast	93.71	202.28	188.24	159.86
Slow	108.24	179.89	249.65	141.35
524				
Fast	72.94	284.34	152.89	153.48
Slow	83.69	250.42	180.94	179.64
1918				
Fast	50.97	268.95	137.94	250.40
Slow	62.22	283.70	114.09	266.71

4.1.2. Desorption rate constants

Desorption rate constants ranged from 7.87 ± 0.60 to 13.17 ± 1.61 y^{-1} for slow-sinking particles, and from 1.81 ± 0.44 to 13.96 ± 0.48 y^{-1} for fast-sinking particles. For comparison, Nozaki et al. (1987) reported desorption rate constants ranging from 0.88 ± 1.2 y^{-1} to 1.89 ± 5.1 y^{-1} in the western Pacific; Bacon et al. (1989) presented results that ranged from 2.6 to 9.8 y^{-1} for the Arctic Ocean; and Bacon and Anderson (1982) reported a range of 1.3–6.3 y^{-1} at the Panama Basin. Murnane et al. (1994) estimated desorption rate constants of 3.1 ± 1.5 y^{-1} in the northwestern Atlantic Ocean. The highest desorption value ever reported is 316 y^{-1} by Lavelle et al. (1991) at the Puget Sound. Thus, our desorption rate constants are in good agreement with previous studies. Our finding that slow-sinking particles have both higher adsorption and desorption rate constants than fast-sinking particles suggests that slow-sinking particles have more intense interactions with thorium than fast sinking particles.

4.1.3. Remineralization

Remineralization rate constants in this study are lower than those reported in Clegg et al. (1991), who presented a value of 1.64 y^{-1} below 200 m and a decreasing trend with depth. Our estimate for the lower layer (0.51 y^{-1}) is consistent with the value reported by Clegg et al. while the value at the upper layer (1.74×10^{-3} y^{-1}) may be low. The counter-intuitive distribution could be owing to the nature of the data. The particle mass collected in the slow-sinking class at 313 m is similar to that at 524 m, but there is a decrease between 524 m and 1918 m.

4.1.4. Aggregation and disaggregation

In contrast to the results reported by Clegg et al. (1991) that showed aggregation and disaggregation rate constants decreasing with depth, our results show that aggregation rate constants are indeed higher in the upper layer than the lower layer, but disaggregation rate constant are lower in the upper layer than the lower layer. The distribution pattern of aggregation rate constants could be due to the fact that decomposition of organic matter (Table 4) makes particles less sticky in the lower layer than the upper layer, thus the lower layer would have lower aggregation rate constants. The high disaggregation rate constant in the lower

layer could also be explained by decomposition of organic matter: decomposition of the "glue" holding particles together (Armstrong et al., 2002), would leave them vulnerable to breakdown.

For comparison, aggregation and disaggregation rate constants estimated here are lower than the average values estimated in the northwest Atlantic by Murnane et al. (1994), but are comparable with Murnane et al. (1990), in which the rate constants were modeled with data from the North Pacific. Comparisons with other studies (Nozaki et al., 1987; Murnane, 1994) also show comparable aggregation rate constants. Disaggregation rate constants, however, are 2–3 orders of magnitude lower than those in the above citations. The discrepancy between our results and previous studies may be due to geographical differences, or due to the different methods used to estimate the parameters (Wang, 2015). Aggregation and disaggregation fluxes are calculated by multiplying aggregation and disaggregation rate constants with slow- and fast-sinking particle concentrations, respectively. As shown in Table 3, particles do exchange via aggregation, which is in agreement with Abramson et al. (2010), in which aggregation and disaggregation were studied by comparing pigment and amino acid compositions of particles sampled by large volume pumps and sediment traps during the 2005 MedFlux program.

4.1.5. *Explanations for the depth distributions of ^{234}Th flux density*

One inspiration for the current study was to seek an explanation for the flux density distributions of ^{234}Th as reported in Szlosek et al. (2009) and displayed in Fig. 1. For particles that sink very slowly (e.g., 10 m/d), the time for completing the journey from 313 m to 1918 m (depths of the shallowest and the deepest traps) is more than 5 half-lives of ^{234}Th (24.1 days), which means that more than 97% of the ^{234}Th scavenged at 313 m will have been lost by radioactive decay when the particles reach 1918 m. However, Fig. 1 shows that the ^{234}Th flux densities are almost the same at different depths. For fast-sinking particles, the transit time is short compared with the ^{234}Th half-life; we therefore expect that loss by radioactive decay should be negligible, and flux density variations with depth should be small. But Fig. 1 shows that deeper traps exhibit higher ^{234}Th flux densities. Szlosek et al. (2009) concluded that there must be processes that add thorium onto fast sinking particles. Our objective here was to find out which process or processes is (are) responsible.

For sinking particles, there are seven processes that influence the ^{234}Th budget as shown in Fig. 3: adsorption, desorption, remineralization, aggregation, disaggregation, sinking flux divergence, and radioactive decay. Their contributions to the budget are shown in Table 3. For slow-sinking particulate ^{234}Th, loss by radioactive decay and desorption are mainly compensated by adsorption of dissolved ^{234}Th. Slow-sinking particulate ^{234}Th is also lost by particle sinking and aggregation, but the two processes together contribute only about 10–20% of the loss by radioactive decay and desorption. We conclude that, for slow-sinking particulate ^{234}Th, adsorption is the major process responsible for compensating the loss by radioactive decay. For fast-sinking particulate ^{234}Th, the loss by radioactive decay is relatively small. Vertical flux contributes about 50–90% of the sink. The loss from disaggregation is negligible at the upper layer, and accounts for ~10% of the total loss at the lower layer. Adsorption accounts for ~60%, and aggregation contributes the remaining ~40% of the gain in ^{234}Th on fast-sinking particles. We conclude that a combination of adsorption and aggregation is responsible for adding ^{234}Th to the fast-sinking particles (Fig. 1).

These results have significance for understanding the controls on the ratio of particulate organic carbon to ^{234}Th (POC/Th) that is used commonly to calculate POC fluxes from ^{234}Th deficits in the water column. Cai et al. (2006) proposed that decay of ^{234}Th on sinking particles could alter the POC/Th ratio and produce erroneous POC fluxes. In contrast, our results show that, at least at the DYFAMED site, ^{234}Th decay on sinking particles is not a factor in producing the changes in POC/Th observed there, as described in detail by Szlosek et al. (2009). Instead, other processes such as remineralization, aggregation, and disaggregation are controlling the POC flux on sinking particles (Table 3).

5. Conclusions

By using maximum likelihood estimation, we avoid prescribing prior information that is highly objective, thus we obtain a unique set of estimates that are totally determined by the data. Slow-sinking particles have higher adsorption and desorption rate constants compared to fast-sinking particles. Both adsorption and desorption increase slightly with depth. For the distribution of ^{234}Th flux density observed in the MedFlux project, our explanation is that during the transit of particulate material from the surface ocean to the deep sea, the loss of ^{234}Th by radioactive decay on slow-settling particles is compensated by adsorption, and therefore that the ^{234}Th flux in slow-settling particles captured by the deep trap are approximately the same as those in the shallower traps. In contrast, fast-sinking particles also absorb thorium during sinking, but the loss from radioactive decay is low, which explains why the deep trap has higher ^{234}Th fluxes on rapidly settling particles. Interactions among slow- and fast-settling particle classes through disaggregation are low.

Acknowledgements

This study is part of W. Wang's Ph.D. dissertation. We thank thesis committee members, C. Lee, K. Lwiza (Stony Brook University), and G. Stewart (Queens College, City University of New York) for their valuable suggestions. Support was provided by the Chemical Oceanography Program of the US National Science Foundation (MedFlux 06-22754 and BarFlux 10-61128) and the United Nations International Atomic Energy Agency to their Marine Environmental Studies Laboratory in Monaco. We express our sincere gratitude to two anonymous reviewers for valuable suggestions and efforts that improved this study.

References

Abramson, L., Lee, C., Liu, Z., Wakeham, S.G., Szlosek, J., 2010. Exchange between suspended and sinking particles in the Northwest Mediterranean as inferred from the organic composition of in situ pump and sediment trap samples. Limnol. Oceanogr. 55 (2), 725–739.

Armstrong, R.A., Lee, C., Hedges, J.I., Honjo, S., Wakeham, S., 2002. A new, mechanistic model for organic carbon fluxes in the ocean based on the quantitative association of POC with ballast material. Deep-Sea Res. II 49, 219–236.

Armstrong, R.A., Peterson, M.L., Lee, C., Wakeham, S.G., 2009. Settling velocity spectra and the ballast ratio hypothesis. Deep Sea Res. II 56, 1470–1478.

Bacon, M.P., Anderson, R.F., 1982. Distribution of thorium isotopes between dissolved and particulate forms in the deep sea. J. Geophys. Res. 87, 2045–2056.

Bacon, M.P., 1984. Glacial to interglacial changes in carbonate and clay sedimentation in the Altlantic ocean estimated from 230Th measurements. Isot. Geosci. 2, 97–111.

Bacon, M.P., Huh, C.A., Moore, R.M., 1989. Vertical profiles of some natural radionuclides over the Alpha Ridge Arctic Ocean. Earth Planet. Sci. Lett. 95, 15–22.

Barnett, T.P., Adam, J.C., Lettenmaier, D.P., 2005. Potential impactes of a warming climate on water availability in snow-dominated regions. Nature 438, 303–309.

Bourne, M.D., Thomas, A.L., Niocaill, C.M., Henderson, G.M., 2012. Improved determination of marine sedimentation rates using 230Thxs. Geochem. Geophys. Geosyst. 13 (1). http://dx.doi.org/10.1029/2012GC004295.

Buesseler, K.O., 1998. The decoupling of production and particulate export in the surface ocean. Glob. Biogeochem. Cycles 12 (2), 297–310.

Cai, P., Dai, M., Chen, W., Tang, T., Zhou, K., 2006. On the importance of the decay of ^{234}Th in determing size-fractionated C/^{234Th} ratio on marine particles. Geophys. Res. Lett. 33, L23602.

Chen, J.H., Edwards, R.L., Wasserburg, G.J., 1986. ^{238}U, ^{234}U, and ^{232}Th in seawater.

Earth Planet. Sci. Lett. 80, 241–251.
Chuang, C.Y., Santschi, P.H., Wen, L.S., Guo, L., Xu, C., Zhang, S., Jiang, Y., Ho, Y.F., Schwehr, K.A., Quigg, A., Hung, C.C., 2014. Binding of Th, Pa, Pb, Po, and Be radionuclides to marine colloidal macromolecular organic matter. Mar. Chem. . http://dx.doi.org/10.1016/j.marche$10.2014.10.014
Clegg, S.L., Whitfield, M., 1991. A generalized model for the scavenging of trace metals in the open ocean, II, thorium scavenging. Deep Sea Res. Part A 38, 91–120.
Clegg, S.L., Bacon, M.P., Whitfield, M., 1991. Application of a generalized scavenging model to thorium isotope and particle data at equatorial and high-latitude sites in the Pacific Ocean. J. Geophys. Res. 96 (C11), 20655–20670.
Coale, K., Bruland, K., 1985. ^{234}Th and ^{238}U disequilibra within the California current. Limnol. Oceanogr. 32 (2), 189–200.
Cochran, J.K., Buesseler, K.O., Bacon, M.P., Livingston, H., 1993. Thorium isotopes as indicators of particle dynamics in the upper ocean: results from the JGOFS North Atlantic Bloom Experiment. Deep-Sea Res. I 40, 1569–1595.
Cochran, J.K., Buesseler, K.O., Bacon, M.P., Wang, H.W., Hirschberg, D.J., Ball, L., Andrews, J., Crossin, G., Fleer, A., 2000. Short-lived thorium isotopes (234Th, 228Th) as indicators of POC export and particle cycling in the Ross Sea, Southern Ocean. Deep-Sea Res. II 47, 3451–3490.
Cochran, J.K., Miquel, J.C., Armstrong, R.A., Fowler, S.W., Masque, P., Gasser, B., Hirschberg, D., Szlosek, J., Rodriguezy Baena, A.M., Verdeny, E., Stewart, G.M., 2009. Time-series measurement of ^{234}Th in water column and sediment trap samples from the Northwest Mediterranean Sea. Deep Sea Res. II 56 (18), 1487–1501.
Doney, S.C., Fabry, V.J., Feely, R.A., Kleypas, J.A., 2009. Ocean acidification: the other CO_2 problem. Annu. Rev. Mar. Sci. 1, 169–192.
Edwards, A.W.F., 1992. Likelihood. Johns Hopkins University Press, Baltimore, MD.
Feely, R., Sabine, C., Takahashi, T., Wanninkhof, R., 2001. Uptake and storage of carbon dioxide in the oceans: the global CO_2 survey. Oceanography 14 (4), 18–32.
Fleisher, M., Anderson, R., 2003. Assessing the collection efficiency of Ross Sea sediment traps using 230Th and 231Pa. Deep-Sea Res. II 50, 693–712.
Hilborn, R., Mangel, M., 1997. The Ecological Detective: Confronting Models with Data. Princeton University Press, Princeton, New Jersey, p. 133.
Honeyman, B., Santschi, P., 1989. A Brownian-pumping model for oceanic trace metal scavenging: evidence from Th isotopes. J. Mar. Res. 47, 951–992.
Lavelle, J.W., Cokelet, E.D., Cannon, G.A., 1991. A model study of density intrusions into and circulation within a deep, silled estuary: Puget Sound. J. Geophys. Res. 96 (C6), 16779–16800.
Lee, C., Peterson, M.L., Wakeham, S.G., Armstrong, R.A., Cochran, J.K., Miquel, J.C., Fowler, S.W., Hirschberg, D., Beck, A., Xue, J., 2009. Particulate organic matter and ballast fluxes measured using time-series and settling velocity sediment traps in the northwestern Mediterranean Sea. Deep-Sea Res. II 56, 1420–1436.
Libes, S.M., 1992. An Introduction to Marine Biogeochemistry. Wiley, New York, p. 522.
Marchal, O., Lam, P., 2012. What can paired measurements of Th isotope activity and particle concentration tell us about particle cycling in the ocean? Geochim. Cosmochim. Acta 90, 126–148.
McDonnell, A.M.P., Buesseler, K.O., 2010. Variability in the average sinking velocity of marine particles. Limnol. Oceanogr. 55 (5), 2085–2096.
Metropolis, N., Rosenbluth, A.W., Rosenbluth, M.N., Teller, A.H., Teller, E., 1953. Equation of state calculations by fast computing machines. J. Chem. Phys. 21, 1087–1092.
Murnane, R.J., Sarmiento, J.L., Bacon, M.P., 1990. Thorium isotopes, particle cycling models, and inverse calculations of model rate constants. J. Geophys. Res. 95 (C9), 16195–16206.
Murnane, R.J., 1994. Determination of thorium and particle matter cycling parameters at station P: a reanalysis and comparison of least squares techniques. J. Geophys. Res. 99 (C2), 3393–3405.
Murnane, R.J., Cochran, J.K., Sarmiento, J.L., 1994. Estimates of particle- and thorium- rates in the Northwest Atlantic Ocean. J. Geophys. Res. 99 (C2), 3373–3392.
Murnane, R.J., Cochran, J.K., Buesseler, K.O., Bacon, M.P., 1996. Least-squares estimates of thorium, particle, and nutrient cycling rate constants from the JGOFS North Atlantic Bloom Experiment. Deep-Sea Res. I 43 (2), 239–258.
Nozaki, Y., Horibe, Y., Tsubota, H., 1981. The water column distribution of thorium isotopes in the western north pacific. Earth Planet Sci. Lett. 54, 203–216.
Nozaki, Y., Yang, J.S., Yamada, M., 1987. Scavenging of thorium in the ocean. J. Geophys. Res. 92, 772–778.
Owens, S.A., Buesseler, K.O., Sims, K.W.W., 2011. Re-evaluating the ^{238}U-salinity relationship in seawater: implications for the 238U-234Th disequilibrium method. Mar. Chem. 127 (1–4), 31–39.
Peterson, M.L., Thoreson, D.S., Hedges, J.I., Lee, C., Wakeham, S.G., 1993. Filed evaluation of a valved sediment trap. Limnol. Oceanogr. 38, 1741–1761.
Peterson, M.L., Wakeham, S.G., Lee, C., Askea, M., Miquel, J.C., 2005. Novel techniques for collection of sinking particles in the ocean and determining their settling rates. Limnol. Oceanogr. Methods 3, 520–532.
Peterson, M.L., Fabres, J., Wakeham, S.G., Lee, C., Alonso, I.J., Miquel, J.C., 2009. Sampling the vertical particle flux in the upper water column using a large diameter free-drifting NetTrap adapted to an Indented Rotating Sphere sediment trap. Deep Sea Res. II 56, 1547–1557.
Press, W.H., Flannery, B.P., Teukolsky, S.A., Vetterling, W.T., 1986. Numerical Recipes. Cambridge University Press, Cambridge, England.
Quigley, M.S., Santschi, P.H., Hung, C.C., Guo, L., Honeyman, B.D., 2002. Importance of acid polysaccharides for ^{234}Th complexation to marine organic matter. Limnol. Oceanogr. 47 (2), 367–377.
Roy-Barman, M., Coppola, L., Souhaut, M., 2002. Thorium isotopes in the western Mediterranean Sea: an insight into the marine particle dynamics. Earth Planet. Sci. Lett. 196, 161–174.
Roy-Barman, M., Lemaitre, C., Ayrault, S., Jeandel, C., Souhaut, M., Miquel, J.C., 2009. The influence of particle composition on thorium scavenging in the Mediterranean Sea. Earth Planet. Sci. Lett. 286, 526–534.
Santschi, P., Li, Y., Bell, J., 1979. Natural radionuclides in the water of Narragansett Bay. Earth Planet. Sci. Lett. 45, 201–213.
Santschi, P.H., Murray, J.W., Baskaran, M., Benitez-Nelson, C.R., Guo, L.D., Hung, C.-C., Lamborg, C., Moran, S.B., Passow, U., Roy-Barman, M., 2006. Thorium speciation in seawater. Mar. Chem. 100, 250–268.
Siegenthaler, U., Sarmiento, J., 1993. Atmospheric carbon dioxide and the ocean. Nature 365, 119–125.
Szlosek, J., Cochran, J.K., Miquel, J.C., Masque, P., Armstrong, R.A., Fowler, S.W., Gasser, B., Hirschberg, D.J., 2009. Particulate organic carbon-^{234}Th relationships in particles separated by settling velocity in the Northwest Mediterranean Sea. Deep Sea Res. II 56, 1519–1532.
Volk, T., Hoffert, M.I., 1985. Ocean carbon pumps: analysis of relative strengths and efficiencies in ocean-driven atmospheric CO_2 changes. Geophys. Monogr. Ser. 32, 99–110.
Wakeham, S.G., Lee, C., 1993. Production, transport, and alteration of particulate organic matter in the marine water column. In: Engel, M.H., Macko, S.A. (Eds.), Organic Geochemistry. Plenum Press, New York, pp. 145–169.
Wang, W., 2015. Using Geochemical Tracers and Mathematical Models to Estimate Sinking Particle Interaction Rate Constants. Stony Brook University, Stony Brook, NY.
Xue, J., Armstrong, R.A., 2009. An improved “benchmark” method for estimating particle settling velocities from time-series sediment trap fluxes. Deep Sea Res. II 56 (18), 1479–1486.